THE JOURNAL OF PHYSICAL CHEMISTRY B

Article

Cite This: J. Phys. Chem. B 2019, 123, 6303−6313

pubs.acs.org/JPCB

# Understanding the Phase and Morphological Behavior of Dispersions of Synergistic Dual-Stimuli-Responsive Poly(*N*-isopropylacrylamide) Nanogels

Adam Town,[†] Edyta Niezabitowska,[†] Janine Kavanagh,[§] Michael Barrow,[∥] Victoria R. Kearns,[⊥] Esther García-Tuñón,[‡] and Tom O. McDonald*[,†]

[†]Department of Chemistry & Materials Innovation Factory and [‡]School of Engineering & Materials Innovation Factory, University of Liverpool, Oxford Street, Liverpool L69 7ZD, U.K.

[§]Department of Earth, Ocean and Ecological Sciences, University of Liverpool, Jane Herdman Laboratories, Liverpool L69 3GP, U.K.

[∥]Anton Paar (UK) Ltd., Unit F, The Courtyard, St. Albans AL4 0LA, U.K.

[⊥]Department of Eye and Vision Science, University of Liverpool, Liverpool L7 8TX, U.K.

Supporting Information

**ABSTRACT:** This work represents a detailed investigation into the phase and morphological behavior of synergistic dual-stimuli-responsive poly(*N*-isopropylacrylamide) nanogels, a material that is of considerable interest as a matrix for in situ forming implants. Nanogels were synthesized with four different diameters (65, 160, 310, and 450 nm) as monodispersed particles. These different samples were then prepared and characterized as both dilute (0.1 wt %) and concentrated dispersions (2−22 wt %). In the dilute form, all of the nanogels had the same response to the triggers of the physiological temperature and ionic strength. In water, the nanogels would deswell when heated above 32 °C, while they would aggregate if heated above this temperature at the physiological ionic strength. In the concentrated form, the nanogels exhibited a wide range of morphological changes, with liquid, swollen gel, shrunken gel, and aggregate structures all possible. The occurrence of these structures was dependent on many factors such as the temperature, ionic strength of the solvent, size and $\zeta$-potential of the nanogel, and dispersion concentration. We explored these factors in detail with techniques such as visual studies, rheology, effective volume fraction, and shape factor measurement. The different-sized nanogels displayed differing phase and morphological behavior, but generally higher concentrations of the nanogels (>7 wt %) yielded gels in water with the transitions depending on the temperature. The smallest nanogel (65 nm diameter) exhibited the most unique behavior; it did not form a swollen gel at any concentration tested. Shape factor measurement for the nanogel samples showed that two of the larger three samples (160 and 310 nm) had core−shell structures with denser core cross-linking, while the smallest nanogel sample displayed a homogeneous cross-linked structure. We hypothesize that the smallest nanogels are able to undergo more extensive interpenetration compared to the larger nanogels, which meant that the smallest nanogel was not able to form a swollen gel. In the presence of salt at 12 wt %, all of the nanogels formed aggregates when heated above 35 °C due to the screening of the electrostatic stabilization by the salt. This work revealed unique behavior of the smallest nanogel with a homogeneous cross-linked structure; its phase and morphological behavior were unlike a particle dispersion, rather these were more similar to those of a branched polymer solution. In total, these findings can be used to provide information about the design of poly(*N*-isopropylacrylamide) nanogel dispersions for different applications where highly specific spatiotemporal control of morphology is required, for example, in the formation of in situ forming implants or for pore blocking behavior.

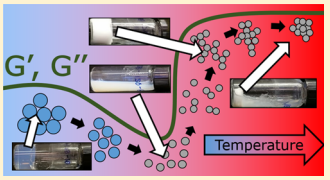


## 1. INTRODUCTION

Nanogels consist of polymers chains that are cross-linked together into a network, forming nanosized particles that swell in a suitable solvent.[1,2] The swelling behavior exhibited by nanogels is stimuli-responsive and can be triggered by changes in properties such as temperature, pH, and solvent. Nanogels have found use in many different practical applications such as surface coatings,[3,4] templates for nanoparticle synthesis,[5] optics,[6,7] and tissue scaffolds.[8] The terms nanogel and microgel are often used interchangeably in the literature, with both terms used widely to describe particles of the same size. Generally, a diameter of 500 nm is the upper limit of what can be classified as a nanogel.[9−13] One particular polymer that has been extensively researched in the form of nanogels is poly(*N*-isopropylacrylamide) (PNIPAm),[14] which was first synthesized in the form of nanogels by Pelton and Chibante.[15] The volume-phase transition temperature (VPTT)[16] of PNIPAm nanogels is around 32 °C, close to the physiological

Received: April 30, 2019
Revised: June 21, 2019
Published: June 28, 2019




DOI: 10.1021/acs.jpcb.9b04051
J. Phys. Chem. B 2019, 123, 6303−6313

temperature of 37 °C.[17−19] Upon heating above 32 °C, the nanogels undergo transition from swollen, hydrophilic particles[8,20] to deswollen particles.[16] This thermal trigger has been used in drug delivery to release drug entrapped within the cross-linked polymer network.[11,21−23] PNIPAm nanogels are also able to undergo morphological transitions such as flocculation upon exposure to dual stimuli of temperature and sufficient ionic strength, a synergistic dual-stimuli-responsive behavior.[24] This flocculation behavior has previously been used with extensive spatiotemporal control to trigger transitions in the nanogels to block membrane pores,[16,25] trigger drug release,[26] as well trigger the formation of an in situ forming implant for drug delivery.[27,28] This flocculation is a phase separation, which is one of the many possible phase and morphological changes that can occur in PNIPAm dispersion.[29] Interestingly, unlike other nanogel dispersions, PNIPAm is able to undergo thermoreversible gelation, transitioning from a liquid to a gel upon temperature switches above and below the VPTT.[30] Other morphological changes such as a gel transition at low temperature and high concentration and colloidal crystal fluids are also possible in PNIPAm-based nanogels.[20,30−32] These morphologies are possible because of the different combinations of colloidal interactions between the nanogels under specific conditions. Below the VPTT, nanogels are sterically stabilized by polymer chain ends, extending out from the particle into solution.[33] However, this steric stabilization is lost above the VPTT as the nanogels deswell. Charges present on the nanogel either from the use of a charged initiator or comonomer can provide electrostatic interaction between the nanogels. This electrostatic repulsion may be screened out by ions present in solution, which can result in nanogel aggregation. Thus, PNIPAm nanogels provide a highly dynamic responsive material for providing on-demand morphological transitions.

The phase and morphological changes of PNIPAm nanogel dispersions have been studied previously using techniques such as visual observations, rheology,[20,30,34−37] microscopy,[35] static and dynamic light scattering (DLS),[38−40] small-angle neutron scattering,[38] differential scanning calorimetry, and turbidimetry.[41] Rheology is a useful and widely used technique for studying the morphological behavior of nanogel dispersions, as the shear storage ($G'$) and shear loss ($G''$) moduli measured by oscillatory rheometry often change dramatically between different morphologies,[12,30,34,36,42] allowing the supplementation of visual observations of morphological transitions more accurately with rheological measurements. The temperature at which the swollen gel-to-liquid transition occurred can be explained by considering the effective volume fraction ($\varphi_{eff}$) of the different nanogels. The effective volume fraction gives a measure of the packing of the nanogels and is both temperature and concentration dependent. An $\varphi_{eff}$ of ∼0.74 is the close packing limiting value for monodispersed hard spheres;[43] when the $\varphi_{eff}$ is greater than this value, the particles are restricted to volumes smaller than their dilute solution equilibrium swelling volumes.[35] Hence, if the spheres are able to compress and deform, a value greater than ∼0.74 can be achieved.[20] This is because $\varphi_{eff}$ does not take into account any effect of deformation, deswelling, or interpenetration of particles on the volume fraction.[44] The effective volume fraction can be estimated using the viscosity of a dilute dispersion and the Batchelor equation.[45,46] Conley et al. used two-color super-resolution microscopy to show that as the concentration of PNIPAm nanogels was increased above a $\varphi_{eff}$ of 0.64 the interpenetration and shape deformation became dominant. As the concentration was increased above $\varphi_{eff}$ of 1.75, the only remaining way to further densify the system was by isotropic compression.[47] Urayama et al. examined the effect of different cross-linking densities (1−5 mol %), sizes of nanogels (350−1550 nm), and $\varphi_{eff}$ values (0.65−1.2) on the yielding behavior of PNIPAm nanogels by rheology. They showed that the yield strain for different samples was nearly insensitive to the cross-linking density, particle diameter, and particle concentration.[48] Senff and Richtering also investigated the effect of cross-linking density in PNIPAm nanogels on rheological properties at temperatures above and below the VPTT. They showed that with the increased cross-linking density (0.6−5.3 mol %) the swelling of the nanogels became more restricted, which resulted in lower relative viscosities.[49] While there have been studies on phase and morphological behavior of PNIPAm nanogels, the phase and morphological behavior of synergistic dual-stimuli-responsive PNIPAm nanogels have not been studied. The potential to use two stimuli as the trigger for morphological changes provides the possibility of extensive spatiotemporal control of morphological behavior.

In this work, we investigate in detail the phase and morphological behavior of synergistic dual-stimuli-responsive nanogels.[27] We have previously shown that the size of nanogels (65−450 nm) influences the rate of drug release from in situ forming implants and the mechanical properties of the implant.[28] We now study the visual morphological changes and rheological properties of nanogels to understand the phase and morphological changes. We anticipated the size of nanogels to have an effect on the properties of the concentrated dispersions, and therefore, we studied nanogels of four different sizes to see the effect of size. The understanding produced by this work will provide information about the design of nanogel synergistic dual-stimuli-responsive nanogel dispersions for different applications.

## 2. EXPERIMENTAL SECTION

**2.1. Materials.** *N*-Isopropylacrylamide (NIPAm, Sigma-Aldrich), *N*,*N*′-methylenebis(acrylamide) (BIS, Sigma-Aldrich), potassium persulfate (KPS, Sigma-Aldrich), phosphate-buffered saline tablets (one tablet dissolved in 200 mL of deionized water yields 0.01 M phosphate buffer, 0.0027 M potassium chloride, and 0.137 M sodium chloride, pH 7.4) (PBS, Fisher Scientific), and sodium dodecyl sulfate (SDS, Sigma-Aldrich) were all used as received. PBS solutions were prepared at pH 7.4 at 1× (137 mM NaCl, 2.7 mM KCl, and 10 mM phosphate-buffered solution). Dialysis was performed with 12−14 kDa and 3.5 kDa MWCO regenerated cellulose membrane dialysis tubing (Spectrum Labs). Type I distilled water obtained from a water purification system had a resistivity of >18 MΩ $cm^{-1}$ (PURELAB option R, Veolia).

**2.2. Synthesis of PNIPAm Nanogels.** The PNIPAm nanogels were synthesized by dispersion polymerization. The NIPAm monomer (7000 mg, 61.9 mmol), BIS cross-linker (700 mg, 4.5 mmol), and SDS surfactant (PNA450 = 30.0 mg, PNA310 = 78.8 mg, PNA160 = 260.2 mg, and PNA65 = 939.1 mg) were dissolved in distilled water (470 mL) in a 1 L two-neck round bottom flask equipped with a stir bar and reflux condenser. This was then sealed and nitrogen was bubbled through the aqueous solution for 1 h while stirring (400 rpm) to remove dissolved oxygen. The solution was then heated to 70 °C. KPS initiator (280 mg) was dissolved separately in distilled water (30 mL) and degassed with $N_2$ for 1 h before


DOI: 10.1021/acs.jpcb.9b04051
J. Phys. Chem. B 2019, 123, 6303−6313

being transferred to the flask containing the monomers. The reaction was maintained under a $N_2$ atmosphere for 4 h at 70 °C before being cooled down to room temperature. The solution was then filtered through glass wool. To remove unreacted impurities, the nanogel suspension was dialyzed for 5 days using regenerated cellulose dialysis tubing (12−14 kDa MWCO for PNA400, PNA310, and PNA160 and 3.5 kDa MWCO for PNA65) (Spectrum Labs), replacing the distilled water every 12 h. The purified suspension was then lyophilized (Virtis Benchtop K with an ultralow-temperature condenser) and stored in a desiccator.

**2.3. Characterization of PNIPAm Nanogels.** The characterization of the nanogels was carried out using dynamic light scattering (DLS) and laser Doppler electrophoresis (LDE). DLS and LDE were performed using a Malvern Zetasizer Nano ZS (running Malvern Zetasizer software V7.12) with 633 nm He−Ne laser, and the detector was positioned at 173°. Dialyzed samples were diluted to 1 mg $mL^{-1}$. The *Z*-average diameter was recorded in the range 15−55 °C using a thermal equilibration time of 600 s in 1 cm path length disposable polystyrene cuvettes. Measurements were repeated in triplicate to give a mean *Z*-average diameter and polydispersity index (PDI). $\zeta$-Potential measurements were performed using DTS1070 folded capillary cells (Malvern, U.K.). The pH of the sample was measured before performing $\zeta$-potential measurements and for all samples fell in the range of 7 ± 0.5. Capillary cells were flushed with ethanol and water prior to usage. The $\zeta$-potential measurement was made with a minimum of 10 and maximum of 40 runs, with a voltage of 150 V. The Smoluchowski approximation was used to calculate the $\zeta$-potential. Due to the tendency of the nanogels to aggregate with increasing ionic strength solution when above 32 °C, the measurements were conducted in the highest stable concentration of 0.001 M NaCl. This is despite the ISO 13099-2:2012 and ASTM E2865-12 standard recommendation of 0.01 M NaCl to avoid potentially inducing electrode polarization, which causes voltage irregularities if solution conductivity is too low. Hence, the $\zeta$-values give a relative qualitative comparison of $\zeta$-potential trends between the samples measured under the same conditions, rather than a quantitative value.

**2.4. Viscosity Measurements.** Lyophilized nanogels were dissolved in water for 24 h on a sample tube roller. PNA400 required 30 min bath sonication (S 100/H, Elmasonic) for complete dispersal. DLS was used to check whether the complete dispersal of lyophilized nanogel was achieved, with particle size and PDI values equivalent to those before lyophilization during the nanogel synthesis; see Table S1. A Poulten Self U-tube Ostwald viscometer (V1618/02) was used to determine the relative viscosity of the dilute aqueous nanogel samples. All viscosity measurements were conducted at 20 ± 0.5 °C and performed in triplicate.

**2.5. Phase, Morphology, and Rheological Studies.** To form nanogel dispersions at different wt % in water and PBS, the lyophilized nanogels were first packed at the bottoms of glass sample vials. Water or PBS was then added to the sample vials, and the samples were held at 20 °C for 30 min to allow the solvent to soak into the lyophilized nanogel material. These samples were held at 27 °C for 24 h to allow the nanogels to completely disperse. The samples were then added to a sonication bath (S 100/H, Elmasonic) for 30 min to remove any trapped air bubbles formed in the high-concentration dispersions. This was repeated up to three times, and the temperature of the bath was kept below 25 °C. For phase and morphology studies, the sample concentrations were increased in 2 wt % intervals from 2 wt % up to the maximum wt % at which each nanogel sample could be homogeneously dispersed: PNA65, 24 wt %; PNA160, 16 wt %; PNA310, 22 wt %; and PNA450, 16 wt %. The nanogel dispersions were heated in 1 °C intervals and allowed to equilibrate for 5 min at each temperature. The phase and morphology of each sample were then observed by visual inspection and the vial inversion method:[50] a liquid flowed down to the bottom of the vial; a swollen gel remained self-supporting and did not flow over 10 s; a shrunken gel remained self-supporting and adhered to the sides of the vial over 10 s with a small excess of water separation visible; an aggregate formed a pellet that was not self-supporting and with a large excess of water phase separation. When a phase or morphology transition occurred between two consecutive temperatures or wt % values, the intermediate value was used. For example, a transition between 10 and 12 wt % is stated to be occurring at 11 wt %. For rheological studies, a Thermo Fischer Haake MARS III rotational rheometer was used with a 35 mm parallel plate geometry to perform oscillatory rheology, and a sample cover and solvent trap were used to prevent water evaporation from the sample. Samples (12 wt %) were loaded into syringes at 33 °C for placement on the rheometer measuring surface as a liquid. The parallel plate geometry head was lowered onto the sample (0.5 mL) and cooled down to 20 °C for 10 min before commencing measurements to erase any loading and stress history. Amplitude sweeps were performed in the range of 0.1−100% strain to find the linear viscoelastic region for each sample, Figure S1. A strain value within the LVE of each sample was selected for the proceeding measurements. This was 1% for PNA450, PNA310, and PNA160 and 20% for PNA65. A time sweep was then conducted for 600 s at fixed strain and frequency values to ensure that $G'$ and $G''$ remained constant over time and to confirm that the sample remained stable under measurement conditions. A dynamic temperature sweep was then performed with a heating rate of 1 °C $min^{-1}$ in the range of 20−45 °C. A frequency of 1 Hz (6.28 rad $s^{-1}$) was used for all measurements as used previously in the literature.[12,36]

**2.6. Characterization of PNIPAm Nanogels by Asymmetric Flow Field Flow Fractionation.** Asymmetric flow field flow fractionation (AF4) experiments were performed on an MT2000 with RI and UV−vis detectors from Postnova Analytics, Landsberg/Germany. A PN3621 multiangle light scattering detector (MALS) with a detector with 21 angles (from 7 to 164°) operating at 532 nm was coupled online to AF4. An autosampler (PN5300) was supplied by Postnova Analytics. The hydrodynamic sizes of the samples were obtained by dynamic light scattering (DLS) using a Zetasizer Nano ZS (running on Malvern Zetasizer software V7.12) (Malvern Instruments, Malvern, U.K.) with 633 nm He−Ne laser and the detector positioned at 173°, coupled online to the MT2000. A 350 $\mu$m spacer and 10 kDa regenerative cellulose membrane were installed in the separation channel. The conditions used for the separations were based on a method existing in the literature.[51] Briefly, the process was as follows; the mobile phase was 0.1 M $NaNO_3$ in Milli-Q $H_2O$. Type I distilled water was obtained from a water purification system and had a resistivity of >18 MΩ $cm^{-1}$ (PURELAB Option R, Veolia). The mobile phase was filtered using a Corning bottle top vacuum filter system with a



DOI: 10.1021/acs.jpcb.9b04051
J. Phys. Chem. B 2019, 123, 6303−6313

**Table 1. Analysis of the Four Nanogel Samples by Dynamic Light Scattering and Electrophoretic Light Scattering in Both Water and PBS at 24 and 40 °C**

| | water at 24 °C | | water at 40 °C | | PBS at 24 °C | PBS at 40 °C |
|---|---|---|---|---|---|---|
| sample | diameter (nm) | ζ-potential (mV)[a] | diameter (nm) | ζ-potential (mV)[a] | diameter (nm) | diameter (nm) |
| PNA65 | 64 | −13 | 38 | −20 | 66 | [b] |
| PNA160 | 165 | −12 | 89 | −30 | 161 | [b] |
| PNA310 | 314 | −18 | 182 | −33 | 325 | [b] |
| PNA450 | 452 | −13 | 267 | −37 | 342 | [b] |

[a]The ζ-potential measurements were obtained in 0.001 M NaCl. [b]All samples aggregated at 33 °C, providing mean sizes that could not be accurately measured by DLS.

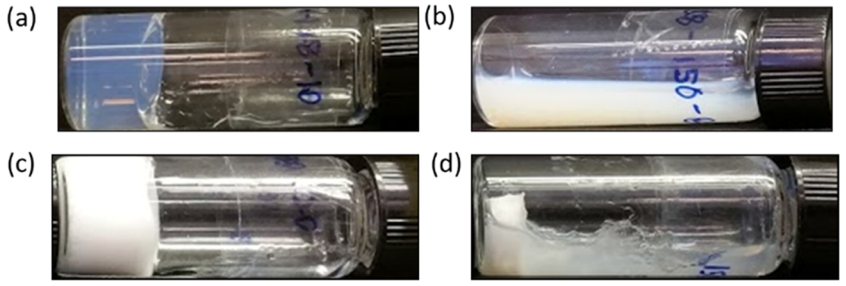


**Figure 1.** Different nanogel phases and morphologies observed in water depending on the temperature: (a) swollen gel (PNA160, 10 wt %, 25 °C), (b) liquid dispersion (PNA160, 10 wt %, 40 °C), (c) shrunken gel (PNA65, 20 wt %, 40 °C), and (d) aggregate (phase separation) (PNA160, 16 wt %, 40 °C).

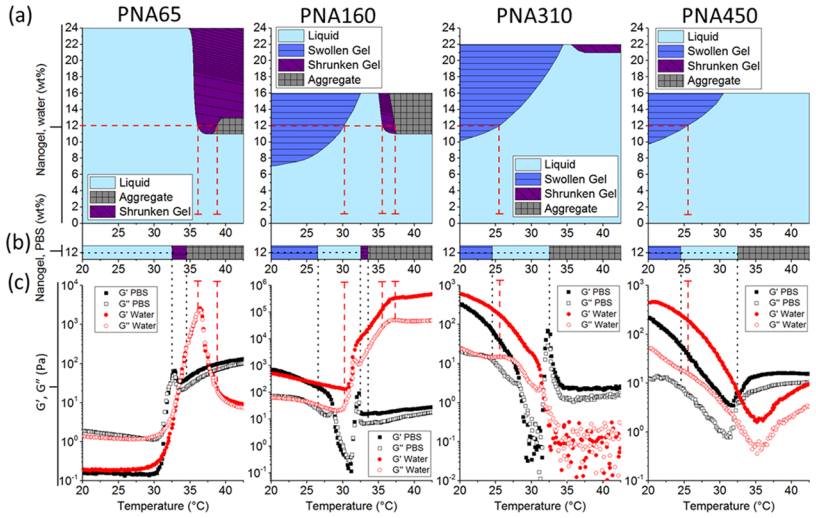


**Figure 2.** Comparison of nanogel phase and morphological behavior and rheological properties in water and PBS at temperatures between 20 and 45 °C for the different nanogel samples with mean diameters from the smallest (left) to the largest (right), 65, 160, 310, and 450 nm, respectively. (a) Phase and morphology diagrams of different nanogel samples dispersed in water at concentrations ranging from 2 wt % up to a maximum of 24 wt %. (b) Phase and morphology diagrams of nanogel samples dispersed in PBS at 12 wt %. (c) Rheological measurements of 12 wt % nanogel dispersions. Lines are a guide for the eye between the changes seen in the phase and morphology diagrams in water (dashed line) and PBS (dotted line) and the rheological data.

cellulose acetate membrane with a pore size of 0.22 μm. The injected volume was 20 μL of 4 mg mL$^{-1}$ sample, as determined by an autosampler. Each sample was analyzed three times to check reproducibility. A blank was measured between injections of new sample to make sure that the system was clean. The UV−vis detector measured two wavelengths at 250 and 300 nm. The conditions used for the separations were as follows: the injection/focusing time was 3 min. The cross flow rate was kept at 1 mL min$^{-1}$ for the first 0.2 min ($t_0$–$t_{0.2}$) in a constant manner, and thereafter, the cross flow was decreased in a power manner (exponent 0.2) to 0.1 mL min$^{-1}$ over a period of 40 min. Following the complete reduction in cross flow, the tip flow of 0.1 mL min$^{-1}$ continued for additional 40 min.

## 3. RESULTS

**3.1. Nanogel Synthesis and Characterization.** Nanogels of four different sizes were synthesized using different amounts of the surfactant sodium dodecyl sulfate (SDS), following the relationship previously reported by Pelton et al.[52] These samples are denoted PNA65, PNA160, PNA310, and PNA450, corresponding to their hydrodynamic diameter in water at 24 °C. The mean diameters and ζ-potential values of the four nanogel samples are shown in Table 1. The *Z*-average



DOI: 10.1021/acs.jpcb.9b04051
J. Phys. Chem. B 2019, 123, 6303−6313

diameter and the polydispersity index of each nanogel as determined by DLS are as follows: PNA65, 63 nm, 0.13; PNA160, 165 nm, 0.02; PNA310, 314 nm, 0.01; and PNA450, 452 nm, 0.03. As expected, all four nanogel samples displayed a change in the hydrodynamic diameter of these nanogels in response to a rise in temperature when dispersed in water. Upon heating above the VPTT of 34 °C, the particles displayed a decrease in diameter and the diameters at 40 °C were between 58 and 69% of the diameters at 25 °C (Table 1). The $\zeta$-potential at 24 °C was similar for all of the samples with the values ranging between −11 and −18 mV. When the nanogels were heated to a temperature of 40 °C, all of the samples became more charged with $\zeta$-potential values between −20 and −37 mV, with a clear trend for samples with larger mean diameters having a greater surface charge.

When the nanogel dispersions were heated in PBS, it was seen that aggregation occurred at 33 °C for all samples and no differences between the aggregation temperatures were observed for the different particles (Table 1).

**3.2. Phase and Morphological Behavior.** To allow direct comparison between the different nanogel samples, their phase and morphological behavior while dispersed in water were investigated in detail. The samples were heated from 20 to 45 °C in 1 °C increments. The temperature-responsive swelling of the nanogels resulted in a wide range of morphological changes with swollen gel, liquid, shrunken gel, and aggregate (phase separation) structures all observed under specific combinations of the nanogel size, concentration, and temperature, as seen in previous works.[53,54] All of the four morphologies are shown using example combinations of nanogel size, concentration, and temperature in Figure 1. At temperatures below the VPTT (<25 °C at 12 wt %), a swollen gel was observed for PNA160, PNA310, and PNA450, which was signified by the presence of a transparent and self-supporting gel (Figure 1a). Turbid liquid dispersions (Figure 1b) were generally observed upon heating the nanogels at temperatures above the VPTT. A shrunken gel (Figure 1c) was observed at temperatures above the VPTT and certain concentrations.[30,55] A phase-separated aggregate was also possible at temperatures above the VPTT, depending on the nanogel sample and its concentration. In this morphology, the nanogels have aggregated in a compact manner and thus no longer form a gel (Figure 1d).

All of the samples revealed different morphologies when dispersed in water, depending on the concentration and temperature (Figure 2a). The smallest nanogel, PNA65, was a liquid at all temperatures tested when the concentration was less than 11 wt %. At concentrations above 11 wt % and temperature above 36 °C, a shrunken gel was generally observed. At concentrations between 11 and 13 wt % and temperature above 38 °C, an aggregate was observed. The three larger nanogel samples PNA160, PNA310, and PNA450 all showed a liquid-to-swollen gel transition, which was dependent on the concentration and temperature; at 20 °C, swollen gels were observed at all concentrations above 7 wt % for PNA160 and 10 wt % for both PNA310 and PNA450. At higher temperatures, an increased concentration of the nanogel was required before a swollen gel was obtained. The PNA160 sample formed a shrunken gel at concentrations above 11 wt % and at 36 °C; and further heating above approximately 37 °C resulted in aggregate formation. The PNA310 sample only formed a shrunken gel above 21 wt % and at temperatures above 36 °C with no aggregate formation observed. The largest nanogel sample, PNA450, displayed no shrunken gel or aggregate morphologies in water at the concentrations tested (Figure 2a).

The morphological behaviors of the four nanogel samples were then tested in PBS at 12 wt %, a concentration selected as it showed morphological changes for all four of the nanogel samples (see Figure 2b). In the presence of PBS, all samples exhibited at least three different morphologies. Samples PNA65 and PNA160 exhibited the same transitions as observed for the sample in water at 12 wt % but with lower transition temperatures. The larger nanogels PNA310 and PNA450 also displayed the liquid-to-swollen gel transition at lower temperatures in PBS compared to when dispersed in water, with the transition temperature changing from 25.5 to 24.5 °C for both samples. Additionally, these larger nanogel samples displayed an additional morphological transition that was not observed in water at 12 wt % with the formation of aggregates at 32.5 °C.

**3.3. Rheological Properties.** Oscillatory rheology was performed on the concentrated nanogel dispersions (12 wt %) in water and PBS, Figure 2c, to compare the rheological properties of the dispersion with the visual phase and morphological behavior in water, Figure 2a, and PBS, Figure 2b. The $G'$ (storage modulus) and $G''$ (loss modulus) values were investigated as these values are the most relevant for studying the morphological behavior of the concentrated nanogel dispersions. The relative proportions of $G'$ and $G''$ are reflected by the phase-shift angle, $\delta$, such that $G''/G' = \tan\delta$. Figure 2c shows that for PNA65, $G''$ was an order of magnitude larger than $G'$ below 30 °C (ca. 1 and 0.1 Pa, respectively). At these conditions, it had $\tan\delta \gg 1$ (Figure S4), indicating that the sample was a viscous liquid, as seen in the phase and morphology study (Figure 2a). Conversely, $G'$ was an order of magnitude greater than $G''$ for PNA160, PNA310, and PNA450 at 20 °C (ca. $10^3$ and $10^2$). For the three larger nanogels, as the temperature was increased, the values for $G'$ and $G''$ gradually decreased and the separation between $G'$ and $G''$ decreased (Figure 2c). The initial values of $G'$ and $G''$ are most significantly lower in PBS compared to those in water for PNA450. In water, the nanogels gave a larger $G'$ value and hence formed a stiffer gel. Before the swollen gel-to-liquid transition, there was also a more gradual decrease of $G'$ and $G''$ than after the transition, where a slightly steeper gradient for $G'$ and $G''$ could be observed for PNA160, PNA310, and PNA450.

In both water and PBS, as the temperature was increased above 30 °C, the visually observed morphology transitions corresponded to abrupt increases in $G'$ and $G''$. These increases were at least 2 orders in magnitude for PNA65, PNA160, and PNA310 and 1 order of magnitude for PNA450 and in the phase and morphology study corresponded with the formation of shrunken gel or aggregate morphologies. In the case of PNA310 in water, the sample remained a liquid at higher temperatures (Figure 2c). In PNA450, there was a less significant and more gradual increase in $G'$ and $G''$ at high temperatures for the aqueous dispersion. After performing the dynamic temperature sweep, small aggregates were observed in the sample, explaining the rise in $G'$ and $G''$ (Figure S5). PNA 65, PNA160, and PNA310 also show a rise in $G'$ and $G''$ (and viscosity, see Figure S6) around the VPTT.

**3.4. Effective Volume Fraction.** The effective volume fraction gives a measure of the packing of the nanogels and is both temperature and concentration dependent. The effective



DOI: 10.1021/acs.jpcb.9b04051
J. Phys. Chem. B 2019, 123, 6303−6313

volume fraction was calculated using the relative viscosity ($\eta_{rel}$) of dilute dispersions of each nanogel and then fitting the Batchelor equation to this data as described previously, Figure 3a (see equations used for calculations in eq S1).[20,35,36,40] It

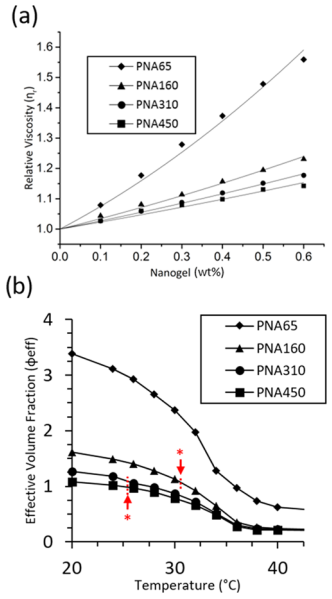


**Figure 3.** Determination of effective volume fraction using the Batchelor equation and viscosimetry data. (a) Relative viscosity data for nanogels measured at 20 °C fitted with the Batchelor equation ($\eta_{rel} = 5.9(kc)^2 + 2.5(kc) + 1$, $\varphi_{eff} = kc$). (b) $\varphi_{eff}$ at 12 (w/w) % nanogel aqueous dispersion across a temperature range. PNA450 (squares), PNA310 (circles), PNA160 (triangles), and PNA65 (diamonds). The swollen gel-to-liquid transition occurs at the dashed line (red asterisk).

can be seen that the relative viscosity of the nanogel is dependent on the nanogel size, with smaller nanogels giving a higher relative viscosity for dispersions formed from the same wt % of the nanogel (Figure 3a).

The effect of temperature on the effective volume fraction for each nanogel as a 12 wt % dispersion can be seen in Figure 3b. The smaller the nanogel, the larger the effective volume fraction. At the temperature of transition from swollen gel to liquid, the effective volume fractions for PNA160, PNA310, and PNA450 are 1.1, 1.1, and 1.0, respectively; see (*) as indicated by the arrow and dashed line in Figure 3b.

**3.5. Internal Structure of the Nanogels.** Asymmetric flow field flow fractionation (AF4) with inline multiangle light scattering (MALS) and DLS instruments provides the opportunity to obtain high-resolution measurements of the radius of gyration, $R_g$, and the hydrodynamic radius, $R_h$, of the four differently sized nanogel samples. The $R_h$ values agreed closely with the mean diameters as measured by batch DLS. The measurement of $R_g$ allowed calculation of the shape factor, $\rho$ ($\rho = R_g/R_h$), which provided information on the internal structure of the sample, Table 2. The PNA450 sample was too large to be measured accurately by DLS in flow.[56] The shape factor of the two larger nanogel samples (PNA160 and PNA310) was in the range 0.58−0.59, which indicates a core−shell-type structure, while the smallest nanogel (PNA65) had the highest shape factor, 0.73, which indicates a more homogeneous internal structure.

**Table 2. Mode Values of $R_{gh}$, $R_{gh}$, and $\rho$ for Nanogels Obtained from AF4-MALS-DLS**

| sample | $R_g$ [nm] | $R_h$ [nm] | $\rho$ |
|---|---|---|---|
| PNA65 | 25.2 ± 0.1 | 34.5 ± 1.0 | 0.71 |
| PNA160 | 41.9 ± 0.1 | 72.5 ± 1.0 | 0.58 |
| PNA310 | 80.0 ± 0.5 | 136.5 ± 0.3 | 0.59 |

## 4. DISCUSSION

The understanding of how the colloidal interactions of these synergistic dual-stimuli-responsive nanogels change with variation of temperature and ionic strength allows us to design colloidal systems with highly specific spatiotemporal control of the phase and morphological behavior. To do this, we first prepared four different PNIPAm nanogel samples (with mean diameters of approximately 65, 160, 310, and 450 nm) (Table 1) by varying the concentration of the surfactant used during dispersion polymerization. With these samples, we wanted to investigate how the size of the particles influenced the formation of different morphologies.

**4.1. Colloidal Behavior of the Nanogels as Dilute Dispersions.** Initially, the nanogels were studied as a dilute dispersions. The nanogels displayed the typical thermoresponsive behavior whereby an increase in the temperature above the VPTT resulted in a reduction in the particle diameter. This behavior occurs as the polymer−solvent hydrogen bonding becomes less favorable and the polymer−polymer interactions dominate. In water, the nanogels are colloidally stabilized below their VPTT by a combination of steric and electrostatic stabilization.[33] Below the VPTT, the nanogels were sterically stabilized by the solvated polymer chains on the surface of the particles[33] and electrostatically stabilized by the surface charge provided by the sulfate groups at the chain ends that were derived from the persulfate initiator.[52] Upon heating above the VPTT, the steric stabilization was likely lost as the solvated surface chains collapsed and any colloidal stability was obtained from the electrostatic repulsion between the particles.[52,57] Thus, in water, the nanogels are stabilized by a combination of steric and electrostatic interactions.

When the nanogels were analyzed as dilute dispersions in PBS, there was generally a slight decrease in the diameter of the nanogels below the VPTT. This reduction in diameter was most pronounced for the largest nanogel PNA450 that showed a 29% reduction in diameter in PBS (Table 1). The increased concentration of ions present in PBS will increase the polarity of the solvent, making it a poorer solvent for the PNIPAm. Additionally, in water, the sulfate groups may provide some swelling due to the electrostatic repulsion within the particles. In the presence of PBS, these charges will be screened by the increased concentration of ions and result in less swelling.[19] During the synthesis of nanogels, growth continues until a charge density large enough to attain colloidal stability is achieved.[33,58] Hence, we expect that PNA450 will contain the highest amount of sulfate groups in each particle and the screening of these charged groups may cause a pronounced shrinkage in diameter. When the nanogels were heated to ≥33 °C in PBS, the nanogels aggregated; the increased ionic strength of the PBS screened the electrostatic repulsion, resulting in aggregation.[24] We found that the aggregation temperature was completely independent of the particle size in a dilute dispersion. This colloidal behavior was purely driven by electrostatic screening; hence, the aggregation occurs at a


DOI: 10.1021/acs.jpcb.9b04051
J. Phys. Chem. B 2019, 123, 6303−6313

lower temperature with the increase in NaCl concentration, Table S2.[59] This result is similar to that of a previous work by Vincent et al.[19] In PBS, all of the nanogel samples were stabilized purely by steric interactions between particles; when this stabilization was lost (heating above the VPTT), the particles would rapidly aggregate.

**4.2. Phase and Morphological Behavior of the Concentrated Nanogels.** To allow a direct comparison between the different nanogel samples, the phase and morphological behavior of the samples dispersed at increasing concentrations in water were investigated in detail. At concentrations greater than 12 wt %, interesting morphological behavior was seen for the nanogels. Heating these concentrated dispersions could trigger transition from a swollen gel to a liquid, to a shrunken gel, and finally to an aggregate. At temperatures below 30 °C, the nanoparticle interaction potential can be considered as purely repulsive[35] with no significant change in the attractive part of the interaction potential. Three samples, PNA160, PNA310, and PNA450, were able to form a swollen gel below the VPTT when the concentration was sufficient. The swollen gel morphology arises due to a volume blocking mechanism of hard sphere theory, in which the nanogels become closely packed without significant deformation.[42,60] If the samples were heated, the nanogels deswelled and the swollen gel would undergo transition into a turbid liquid, as seen in other PNIPAm nanogel dispersions.[61] This transition occurred as the deswollen particles were no longer large enough to form a gel through volume blocking. The increased turbidity occurred due to the increased difference between the refractive indexes of the nanogel particles and the surrounding liquid. Further heating could also result in a third morphology, a shrunken gel. This morphology was self-supporting but with high turbidity. The shrunken gel morphology was formed due to the increasing tendency of the nanogels to become more hydrophobic and to prefer polymer−polymer interactions as opposed to polymer−water hydrogen bonds when the temperature increases. This change in particle−particle interaction favors aggregation;[59,62] however, electrostatic repulsion prevents the occurrence of complete aggregation.[12] This balance of interactions results in the formation of a network structure throughout the continuous phase due to the partial aggregation of the particles. Finally, upon further heating, more extensive aggregation occurs resulting in the complete phase separation of the nanogels and the continuous phase. In this morphology, the nanogels have aggregated in a compact manner and thus no longer form a gel. Thus, changes in the colloidal interactions of the nanogels underpin the different phase and morphological transitions that were observed.

**4.3. Characterization of the Nanogel Phase and Morphological Transitions in Water.** The four different nanogel samples displayed differences in their phase and morphology diagrams in water, both visually and by rheological analysis (Figure 2). The temperature at which transitions were observed by the vial inversion test were generally accompanied by changes in the rheological data, with the four nanogel samples displaying differing rheological properties. Rheology gives useful information regarding the morphological transitions of the different nanogel samples. However, the low values for the moduli of the liquid phase of PNA65 and the heterogeneity of the aggregate morphology mean that these values should be considered in a qualitative manner.

*4.3.1. Formation of the Swollen Gel Morphology.* Below 30 °C, when the values for $G'$ was an order of magnitude greater than those for $G''$, the material is said to be in a gel state. As the value for $G''$ nears that of $G'$, viscous properties of the material begin to dominate and the material is in a liquid state. Conditions for this transition from swollen gel to liquid differed between the samples. The larger nanogels (PNA160, PNA310, and PNA450) showed that as temperature increased a higher concentration of the nanogel was required to obtain a swollen gel. This behavior can be explained by considering the effective volume fraction of the different nanogels (Figure 3). An effective volume fraction of ∼0.74 is the close packing limiting value for monodispersed hard spheres.[63] When the effective volume fraction is greater than this value, the particles are restricted to volumes smaller than their dilute solution equilibrium swelling volumes.[35] However, if the spheres are able to compress and deform, a value greater than this can be achieved.[20] There is considerable evidence of the deformation on PNIPAm nanogels in the literature.[47,64] In the case of our samples, a comparison of the observed morphological transition at 12 wt % (Figure 2a) and the calculation of the effective volume fraction at 12 wt % (Figure 3) show that the transition from swollen gel and liquid occurred at an effective volume fraction of ∼1 for PNA160, PNA310, and PNA450; therefore, any temperature-induced deswelling of the particles that lowered the effective volume fraction below 1 led to a swollen gel-to-liquid transition. This change was observed in the rheology as a more gradual decrease of $G'$ and $G''$, as less volume blocking occurred and the mobility of the nanogels in the dispersion increased. PNA160 showed rather different changes in the moduli, and the visual transition was accompanied by a considerable increase in both moduli with $G' \approx G''$. As the temperature further increased, $G'$ increased faster than $G''$ until a shrunken gel was observed. This behavior might be attributed to some aggregation on the nanogels, resulting in partial network formation, which highlights the importance of using rheology to understand the morphological changes in the samples. Interestingly, the smallest nanogel PNA65 did not display a swollen gel morphology under the conditions tested, as supported by the rheology measurements where $G'' \gg G'$ for the PNA65 sample when it was a liquid. Even at high concentrations (>12 wt %), PNA 65 was still a liquid with an effective volume fraction of more than 1. It has previously been shown that using larger amounts of SDS during the dispersion polymerization route used for nanogels creates smaller and more homogeneous particles,[65] while using less SDS generates larger particles with a more heterogeneous structure that contains a dense gel particle core.[66] This structure was confirmed by the analysis of PNA65, PNA160, and PNA310 by AF4 (Table 2) using DLS and MALS detectors. The smallest nanogel (PNA65) had the highest shape factor, approaching that of a hard sphere (0.77) and indicating homogeneous cross-linking. The larger nanogel samples had much lower values, which indicate that more of the mass was contained at the center of the particles, a higher cross-linking density in the core compared to the shell. Therefore, PNA65 did not possess the core−shell structures that were found for the larger nanogel samples; it is likely that PNA65 was composed of a lower cross-linking density without a dense gel core (Figure 4). Consequently, the PNA65 particles may be able to have more hydrodynamic corona overlap,[36] giving a larger calculated effective volume fraction.[34,41] Bae and Han previously showed that no swollen



DOI: 10.1021/acs.jpcb.9b04051
J. Phys. Chem. B 2019, 123, 6303−6313

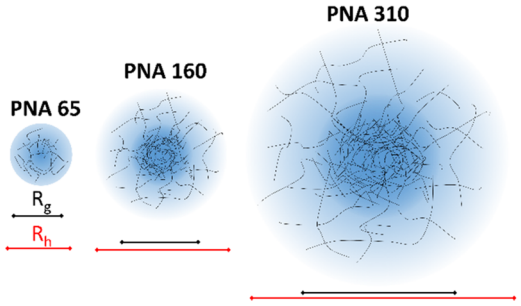


**Figure 4.** Schematic representation of the different internal structures of PNA65, PNA160, and PNA310 based on the $R_g$ and $R_h$ values determined by AF4. The smallest nanogel possessed a homogeneous cross-linking density, while the larger nanogels had a higher cross-linking density at the core of the particles.

gel morphology was observed for linear polymers at a high concentration.[67] We propose that the PNA65 nanogels are able to undergo large deformations to remain fluid as they behave more like branched polymers than hard spheres.[20]

*4.3.2. Formation of the Shrunken Gel Morphology.* The transitions to the shrunken gel morphology in water as seen for PNA65 and PNA160 also showed different behaviors for the two nanogel samples. It was clear that as the nanogel samples increased in diameter, a greater concentration was required for the shrunken gel to be observed. The transition from liquid to shrunken gel was seen by rheology as a rapid rise of more than an order of magnitude in the moduli over a temperature range of <5 °C for both PNA65 and PNA160, showing an increase in stiffness. In both samples, $G' \approx G''$ and thus the shrunken gel displays both liquid and gel characteristics (Figure 2c). It is likely that the larger nanogels (PNA 310 and PNA 450) did not form shrunken gels because their larger $\zeta$-potentials may have prevented aggregation between the particles unlike the smaller nanogels having lower $\zeta$-potentials that aggregated to form a network structure.

*4.3.3. Formation of the Aggregate Morphology.* The formation of the aggregate morphology was only observed in water for PNA65 and PNA160 (Figure 2b). This transition was not very pronounced by rheology but was generally indicated by $G' > G''$. These smallest nanogels have the greater surface areas per unit volume and as a result interparticle interactions will be more prevalent. These increased interactions may result in increased aggregation and the formation of the aggregate morphology for the smallest nanogel samples. These data show that changes in the colloidal stabilization of the particles in water control the morphologies of the material.

**4.4. Characterization of the Nanogel Phase and Morphological Transitions in PBS.** Dispersing the nanogels in PBS rather than in water and heating resulted in different morphological behaviors (Figure 2b); the morphology transitions occurred at lower temperatures and aggregates were observed for all four samples. Analysis of the samples by rheology showed that the values and the trend of $G'$ and $G''$ at temperatures between 20 and 27 °C are similar in both water and PBS. The two larger nanogel samples (PNA310 and PNA450) display lower moduli in PBS compared to that in water, mirroring the decrease in the hydrodynamic diameter measured via DLS (Table 1). In water, the nanogels were more swollen and thus more closely packed compared to those in the PBS experiments and therefore gave a larger $G'$ value and hence form a stiffer gel. The difference in morphological transitions of the nanogels in PBS was likely driven by two main factors. First, the increased polarity of the PBS solution will reduce the temperature at which polymer−polymer interactions dominate. Second, the ions in the PBS will screen the charges of the sulfate groups that provided electrostatic repulsion to the nanogels in water. At the highest temperatures tested, all samples produced a phase-separated aggregate due to the lack of any colloidal stabilization. This behavior is similar to that shown by Hu et al., where a shrunken gel was formed, but if the electrostatic repulsion was screened, then the sample would undergo phase separation and form an aggregate.[30] In our work, only the two smallest nanogel samples displayed a shrunken gel morphology in PBS and this was only found over a narrow temperature range. It is likely that when electrostatic repulsion has been screened out, a shrunken gel can only form when the particles still retain some steric stabilization below the lower critical solution temperature.

In both water and PBS, as the temperature was increased to above 30 °C, the visually observed morphological transitions to a shrunken gel or an aggregate corresponded to abrupt increases in $G'$ and $G''$. These increases were at least 2 orders of magnitude for PNA65, PNA160, and PNA310 and 1 order of magnitude for PNA450 and corresponded to the formation of a shrunken gel or an aggregate in the phase and morphology study. This was observed previously by Xu et al. in the formation of a shrunken gel.[23] The rise in $G'$ and $G''$ corresponds to the increasing attractive interaction between particles as they become more hydrophobic and undergo transition from a liquid to either a shrunken gel or an aggregate morphology. In the case of PNA310 in water, the sample remains a liquid at higher temperatures (Figure 2c). In PNA450, there was a less significant and more gradual increase in $G'$ and $G''$ at high temperatures for the aqueous dispersion, which may be due to shear-induced aggregation of the particles.[68] After performing the dynamic temperature sweep, small aggregates were observed in the sample, explaining the rise in $G'$ and $G''$ (Figure S5). PNA65, PNA160, and PNA310 also show a jump in $G'$ and $G''$ (and viscosity, see Figure S6) around the VPTT. This may be due to shear-induced chain entanglement.[39] We can conclude that it is possible to monitor the morphological transitions of the nanogel dispersions by tracking the change in $G'$ and $G''$ over a temperature range.

**4.5. Relationship between Colloidal Stability and the Morphological Behavior.** The relation between morphological behavior and rheological moduli behavior is summarized in Figure 5, where the formation of the different morphologies was dependent on temperature, as well as on nanogel size (and hence structure) and ionic strength, while the change in moduli can be predicted by trends how $G'$ and $G''$ change with the increasing temperature. For the three larger nanogels at temperature less than 30 °C, the nanogels are sterically stabilized and form a self-supporting gel through volume blocking. As the temperature is increased, the particles begin to deswell and the moduli also decrease as the effective volume fraction decreases. In water, the moduli continue to decrease as the particles further deswell and a liquid is formed. In the presence of PBS, electrostatic repulsion is screened and the particles partially aggregate to form a network (increasing $G'$ and $G''$) as a swollen gel. Further heating can result in the formation of an aggregate. The smallest nanogel sample PNA65 displayed different behavior at low temperatures; this was the most homogeneously cross-linked nanogel. As such, it


DOI: 10.1021/acs.jpcb.9b04051
J. Phys. Chem. B 2019, 123, 6303−6313

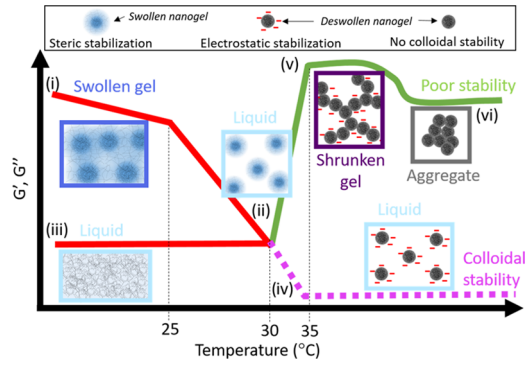


**Figure 5.** Schematic representation of the phase and morphological behavior and changes in rheological moduli of the concentrated nanogel dispersions, as well as the type of stabilization present. Depending on the nanogel size and the concentration and ionic strength of the solvent, different pathways are taken through the different morphologies as the temperature increases. The three larger nanogels (PNA160, PNA310, and PNA450) form swollen gels below 25 °C due to the volume blocking mechanism (i), $G' > 10G''$. Heating these nanogels resulted in a liquid as the particles are no longer large enough to form a gel through volume blocking and the particles are sterically stabilized (ii), $G'G''$ (35 °C) > $10G'G''$ (30 °C). PNA65 was a liquid at all temperatures below the VPTT as the nanogel behaves in a similar manner to a solution of a branched polymer (iii), $G'' > 10G'$. Heating the nanogels above the VPTT could result in two different behaviors, depending on the colloidal stability that was heavily influenced by the solvent. If the nanogels had sufficient colloidal stability through electrostatic repulsion, then the sample remained a liquid (iv), $G'G'' < 0.1$ Pa. In PBS, the nanogels were not completely colloidally stable and further heating could result in partial aggregation, leading to the network formation observed as a shrunken gel morphology (v), $G'G''$ (45 °C) < $10G'G''$ (35 °C). Further heating would result in loss of the remaining colloidal stability and complete aggregation (vi). In water, two smallest nanogels (PNA65 and PNA160) also displayed the behavior associated with poor colloidal stability; in these cases, the high surface area-to-volume ratio of the particles likely resulted in increased particle-particle attractive interactions.

may be able to interpenetrate and behave more like a branched polymer solution rather than a dispersion. Therefore, in PNA65, the volume blocking and particle jamming behaviors do not occur and as a result $G'$ and $G''$ are low.

## 5. CONCLUSIONS

In this work, we have provided a deep insight into factors that control the formation of different morphologies for PNIPAm synergistic dual-stimuli-responsive nanogels. This was achieved through the combined use of visual studies on morphological changes, measurement of the rheological properties, determination of effective volume fraction, and characterization of the internal structure of the nanogels. In a concentration form, the PNIPAm nanogels can display four different morphologies: swollen gel, liquid, shrunken gel, and aggregate morphologies. A complex interaction between the nanogel's surface charge and internal structure and the dispersion conditions (salt concentration, temperature, and nanogel concentration) control the morphological behavior. At low temperatures (below the VPTT), a swollen gel was typically formed due to close packing of the swollen nanogels. At temperatures above the VPTT, volume blocking was lost and a liquid dispersion was formed. Additionally, depending on the colloidal stability of the nanogels, shrunken gel or aggregate morphologies were found above the VPTT. The formation of these morphologies was linked to the surface charge. A high $\zeta$-potential suggests that the nanogels will remain in the liquid morphology, whereas an intermediate value suggests that a shrunken gel morphology will occur followed by an aggregate form as the temperature increases further.

The smallest and most homogeneously cross-linked nanogel prepared displayed rather different properties to those of the larger nanogels. It did not form a swollen gel at any concentration tested, which suggested that these nanogels might behave more like a branched polymer solution rather than a dispersion.

The understanding from this work will help in the development of concentrated PNIPAm nanogel dispersions for different applications, where the triggered formation of different morphologies in response to the ionic strength and temperature may be either desirable or detrimental to the intended application. The well-defined phase and morphological transitions of this system that can be triggered by dual stimuli, which offers the potential for highly specific spatiotemporal control. This material may be of considerable use for pore blocking properties or may be used as a matrix for an in situ forming implant.

## ■ ASSOCIATED CONTENT

### Supporting Information

The Supporting Information is available free of charge on the ACS Publications website at DOI: 10.1021/acs.jpcb.9b04051.

*Z*-Average diameter and PDI of nanogels, amplitude sweep for each nanogel sample, tyndall scattering in PNA160, swelling ratio of nanogels, dynamic temperature sweep tan $\delta$ values, aqueous samples at 50 °C after dynamic temperature sweep, and aggregation temperature of nanogels (PDF)

## ■ AUTHOR INFORMATION


### Corresponding Author

*E-mail: tomm@liv.ac.uk. Tel: +44 (0)151 795 0524.

### ORCID

Tom O. McDonald: 0000-0002-9273-9173


### Notes

The authors declare no competing financial interest.

## ■ ACKNOWLEDGMENTS

We gratefully acknowledge financial support from the EPSRC (Grant numbers EP/M01973X/1, EP/R024839/1, and EP/S012265/1) and a DTA studentship. The authors thank Prof. Steve Rannard for access to equipment and technical support. We are grateful to Prof. Helen Aspinall, Dr. Kate Black, and Josh Turner for access to an Ostwald viscometer.

## ■ REFERENCES

(1) Murray, M. J.; Snowden, M. J. The Preparation, Characterisation and Applications of Colloidal Microgels. *Adv. Colloid Interface Sci.* **1995**, *54*, 73−91.

(2) Baker, W. O. Microgel, a New Macromolecule. Relation to Sol and Gel as Structural Elements of Synthetic Rubber. *Rubber Chem. Technol.* **1949**, *22*, 935−955.

(3) Bradna, P.; Stern, P.; Quadrat, O.; Snuparek, J. Thickening Effect of Dispersions of Ethyl Acrylate-Methacrylic Acid Copolymer Prepared by Different Polymerization Routes. *Colloid Polym. Sci.* **1995**, *273*, 324−330.



DOI: 10.1021/acs.jpcb.9b04051
*J. Phys. Chem. B* 2019, 123, 6303−6313

(4) Boggs, L.; Rivers, M.; Bike, S. Characterization and Rheological Investigation of Polymer Microgels Used in Automotive Coatings. *J. Coat. Technol.* **1996**, *68*, 63−74.
(5) Antonietti, M.; Grohn, F.; Hartmann, J.; Bronstein, L. Nonclassical Shapes of Noble-Metal Colloids by Synthesis in Microgel Nanoreactors. *Angew. Chem., Int. Ed.* **1997**, *36*, 2080−2083.
(6) Xu, S.; Zhang, J.; Paquet, C.; Lin, Y.; Kumacheva, E. From Hybrid Microgels to Photonic Crystals. *Adv. Funct. Mater.* **2003**, *13*, 468−472.
(7) Debord, J. D.; Lyon, L. A. Thermoresponsive Photonic Crystals. *J. Phys. Chem. B* **2000**, *104*, 6327−6331.
(8) Hoare, T. R.; Kohane, D. S. Hydrogels in Drug Delivery: Progress and Challenges. *Polymer* **2008**, *49*, 1993−2007.
(9) Sultana, F.; Manirujjaman; Imran-Ul-Haque; Arafat, M.; Sharmin, S. An Overview of Nanogel Drug Delivery System. *J. Appl. Pharm. Sci.* **2013**, *3*, S95−S105.
(10) Ogawa, K.; Nakayama, A.; Kokufuta, E. Preparation and Characterization of Thermosensitive Polyampholyte Nanogels. *Langmuir* **2003**, *19*, 3178−3184.
(11) Oh, J. K.; Drumright, R.; Siegwart, D. J.; Matyjaszewski, K. The Development of Microgels/Nanogels for Drug Delivery Applications. *Prog. Polym. Sci.* **2008**, *33*, 448−477.
(12) Zhou, G.; Zhao, Y.; Hu, J.; Shen, L.; Liu, W.; Yang, X. A New Drug-Loading Technique with High Efficaciency and Sustained-Releasing Ability via the Pickering Emulsion Interfacial Assembly of Temperature/PH-Sensitive Nanogels. *React. Funct. Polym.* **2013**, *73*, 1537−1543.
(13) Raemdonck, K.; Demeester, J.; De Smedt, S. Advanced Nanogel Engineering for Drug Delivery. *Soft Matter* **2009**, *5*, 707−715.
(14) Schild, H. G. Poly (N-Isopropylacrylamide): Experiment, Theory and Application. *Prog. Polym. Sci.* **1992**, *17*, 163−249.
(15) Pelton, R. H.; Chibante, P. Preparation of Aqueous Latices with N-Isopropylacrylamide. *Colloids Surf.* **1986**, *20*, 247−256.
(16) Mohsen, R.; Vine, G. J.; Majcen, N.; Alexander, B. D.; Snowden, M. J. Characterization of Thermo and PH Responsive NIPAM Based Microgels and Their Membrane Blocking Potential. *Colloids Surf., A* **2013**, *428*, 53−59.
(17) Obeso-Vera, C.; Cornejo-Bravo, J. M.; Serrano-Medina, A.; Licea-Claverie, A. Effect of Crosslinkers on Size and Temperature Sensitivity of Poly(N-Isopropylacrylamide) Microgels. *Polym. Bull.* **2013**, *70*, 653−664.
(18) Kratz, K.; Lapp, A.; Eimer, W.; Hellweg, T. Volume Transition and Structure of Triethyleneglycol Dimethacrylate, Ethylenglykol Dimethacrylate, and N,N′-Methylene Bis-Acrylamide Cross-Linked Poly(N-Isopropyl Acrylamide) Microgels: A Small Angle Neutron and Dynamic Light Scattering Study. *Colloids Surf., A* **2002**, *197*, 55−67.
(19) Rasmusson, M.; Vincent, B. Flocculation of Microgel Particles. *React. Funct. Polym.* **2004**, *58*, 203−211.
(20) Senff, H.; Richtering, W. Temperature Sensitive Microgel Suspensions: Colloidal Phase Behavior and Rheology of Soft Spheres. *J. Chem. Phys.* **1999**, *111*, 1705−1711.
(21) Zhang, X. X.; Lü, S.; Gao, C.; Chen, C.; Zhang, X. X.; Liu, M. Highly Stable and Degradable Multifunctional Microgel for Self-Regulated Insulin Delivery under Physiological Conditions. *Nanoscale* **2013**, *5*, 6498−6506.
(22) Yang, H.; Wang, Q.; Huang, S.; Xiao, A.; Li, F.; Gan, L.; Yang, X. Smart PH/Redox Dual-Responsive Nanogels for On-Demand Intracellular Anticancer Drug Release. *ACS Appl. Mater. Interfaces* **2016**, *8*, 7729−7738.
(23) Qian, K.; Ma, Y.; Wan, J.; Geng, S.; Li, H.; Fu, Q.; Peng, X.; Kan, X.; Zhou, G.; Liu, W.; Xiong, B.; Zhao, Y.; Zheng, C.; Yang, X.; Xu, H. The Studies about Doxorubicin-Loaded p(N-Isopropyl-Acrylamide-Co-Butyl Methylacrylate) Temperature-Sensitive Nanogel Dispersions on the Application in TACE Therapies for Rabbit VX2 Liver Tumor. *J. Controlled Release* **2015**, *212*, 41−49.
(24) Rasmusson, M.; Routh, A.; Vincent, B. Flocculation of Microgel Particles with Sodium Chloride and Sodium Polystyrene Sulfonate as a Function of Temperature. *Langmuir* **2004**, *20*, 3536−3542.
(25) Snowden, M.; Morgan, J.; Vincent, B. A Novel Method for the Enhanced Recovery of Oil. UK Patent GB2262117A, 1993.
(26) Kjøniksen, A. L.; Calejo, M. T.; Zhu, K.; Cardoso, A. M. S.; De Lima, M. C. P.; Jurado, A. S.; Nyström, B.; Sande, S. A. Sustained Release of Naltrexone from Poly(N-Isopropylacrylamide) Microgels. *J. Pharm. Sci. A* **2014**, *103*, 227−234.
(27) Town, A. R.; Giardiello, M.; Gurjar, R.; Siccardi, M.; Briggs, M. E.; Akhtar, R.; McDonald, T. O. Dual-Stimuli Responsive Injectable Microgel/Solid Drug Nanoparticle Nanocomposites for Release of Poorly Soluble Drugs. *Nanoscale* **2017**, *9*, 6302−6314.
(28) Town, A. R.; Taylor, J.; Dawson, K.; Niezabitowska, E.; Elbaz, N. M.; Corker, A.; Garcia-Tuñón, E.; McDonald, T. O. Tuning HIV Drug Release from a Nanogel-Based in Situ Forming Implant by Changing Nanogel Size. *J. Mater. Chem. B* **2019**, *7*, 373−383.
(29) Romeo, G.; Fernandez-Nieves, A.; Wyss, H. M.; Aciernoand, D.; Weitz, D. A. Temperature-Controlled Transitions between Glass. Liquid, and Gel States in Dense p-NIPA Suspensions. *Adv. Mater.* **2010**, *22*, 3441−3445.
(30) Zhou, J.; Wang, G.; Zou, L.; Tang, L.; Marquez, M.; Hu, Z. Viscoelastic Behavior and in Vivo Release Study of Microgel Dispersions with Inverse Thermoreversible Gelation. *Biomacromolecules* **2008**, *9*, 142−148.
(31) Hu, Z.; Xia, X. Hydrogel Nanoparticle Dispersions with Inverse Thermoreversible Gelation. *Adv. Mater.* **2004**, *16*, 305−309.
(32) Xiong, W.; Gao, X.; Zhao, Y.; Xu, H.; Yang, X. The Dual Temperature/PH-Sensitive Multiphase Behavior of Poly(N-Isopropylacrylamide-Co-Acrylic Acid) Microgels for Potential Application in in Situ Gelling System. *Colloids Surf., B* **2011**, *84*, 103−110.
(33) Pelton, R. Temperature-Sensitive Aqueous Microgels. *Adv. Colloid Interface Sci.* **2000**, *85*, 1−33.
(34) Wang, H.; Wu, X.; Zhu, Z.; Liu, C. S.; Zhang, Z. Revisit to Phase Diagram of Poly(N-Isopropylacrylamide) Microgel Suspensions by Mechanical Spectroscopy. *J. Chem. Phys.* **2014**, *140*, No. 024908.
(35) St. John, A. N.; Breedveld, V.; Lyon, L. A. Phase Behavior in Highly Concentrated Assemblies of Microgels with Soft Repulsive Interaction Potentials Phase Behavior in Highly Concentrated Assemblies of Microgels with Soft Repulsive Interaction Potentials. *J. Phys. Chem. B* **2007**, 7796−7801.
(36) Shu, R.; Sun, W.; Liu, Y.; Wang, T.; Wang, C.; Liu, X.; Tong, Z. The Jamming and Unjamming Transition in Poly(N-Isopropylacrylamide) Microgel Suspensions. *Colloids Surf., A* **2013**, *436*, 912−921.
(37) Zhao, Y.; Cao, Y.; Yang, Y.; Wu, C. Rheological Study of the Sol - Gel Transition of Hybrid Gels. *Macromolecules* **2003**, 855−859.
(38) Kratz, K.; Hellweg, T.; Eimer, W. Structural Changes in PNIPAM Microgel Particles as Seen by SANS, DLS, and EM Techniques. *Polymer* **2001**, *42*, 6631−6639.
(39) Howe, A. M.; Desrousseaux, S.; Lunel, L. S.; Tavacoli, J.; Yow, H. N.; Routh, A. F. Anomalous Viscosity Jump during the Volume Phase Transition of Poly(N-Isopropylacrylamide) Particles. *Adv. Colloid Interface Sci.* **2009**, *147−148*, 124−131.
(40) Tan, B. H.; Pelton, R. H.; Tam, K. C. Microstructure and Rheological Properties of Thermo-Responsive Poly(N-Isopropylacrylamide) Microgels. *Polymer* **2010**, *51*, 3238−3243.
(41) Woodward, N. C.; Chowdhry, B. Z.; Snowden, M. J.; Leharne, S. A.; Griffiths, P. C.; Winnington, A. L. Calorimetric Investigation of the Influence of Cross-Linker Concentration on the Volume Phase Transition of Poly(N-Isopropylacrylamide) Colloidal Microgels. *Langmuir* **2003**, *19*, 3202−3211.
(42) Kiminta, D. M. Ö.; Luckham, P. F.; Lenon, S. The Rheology of Deformable and Thermoresponsive Microgel Particles. *Polymer* **1995**, *36*, 4827−4831.
(43) Malkin, A. Y.; Isayev, A. I. Cover Material. In *Rheology - Concepts, Methods and Applications*; ChemTec Publishing: Toronto, 2012.


DOI: 10.1021/acs.jpcb.9b04051
*J. Phys. Chem. B* 2019, 123, 6303−6313

(44) Minami, S.; Watanabe, T.; Suzuki, D.; Urayama, K. Rheological Properties of Suspensions of Thermo-Responsive Poly ( N -Isopropylacrylamide ) Microgels Undergoing Volume Phase Transition. *Polym. J.* **2016**, *48*, 1079−1086.
(45) Luo, J.; Yuan, G.; Zhao, C.; Han, C. C.; Chen, J.; Liu, Y. Gelation of Large Hard Particles with Short-Range Attraction Induced by Bridging of Small Soft Microgels. *Soft Matter* **2015**, *11*, 2494−2503.
(46) Batchelor, G. K. The Effect of Brownian Motion on the Bulk Stress in a Suspension of Spherical Particles. *J. Fluid Mech.* **1977**, *83*, 97−117.
(47) Conley, G. M.; Aebischer, P.; Nöjd, S.; Schurtenberger, P.; Scheffold, F. Jamming and Overpacking Fuzzy Microgels: Deformation, Interpenetration, and Compression. *Sci. Adv.* **2017**, *3*, No. e1700969.
(48) Urayama, K.; Saeki, T.; Cong, S.; Uratani, S.; Takigawa, T.; Murai, M.; Suzuki, D. A Simple Feature of Yielding Behavior of Highly Dense Suspensio ns of Soft Micro-Hydrogel Particles. *Soft Matter* **2014**, *10*, 9486−9495.
(49) Senff, H.; Richtering, W. Influence of Cross-Link Density on Rheological Properties of Temperature-Sensitive Microgel Suspensions. *Colloid Polym. Sci.* **2000**, *278*, 830−840.
(50) Jeong, B.; Bae, Y. H.; Kim, S. W. Thermoreversible Gelation of PEG - PLGA - PEG Triblock Copolymer Aqueous Solutions. *Macromolecules* **1999**, *32*, 7064−7069.
(51) Gaulding, J. C.; Smith, M. H.; Hyatt, J. S.; Fernandez-Nieves, A.; Lyon, L. A. Reversible Inter- and Intra-Microgel Cross-Linking Using Disulfides. *Macromolecules* **2012**, *45*, 39−45.
(52) McPhee, W.; Tam, K. C.; Pelton, R. Poly(N-Isopropylacrylamide) Latices Prepared with Sodium DodecylSulfate. *J. Colloid Interface Sci.* **1993**, 24−30.
(53) Wang, Q.; Zhao, Y.; Yang, Y.; Xu, H. Thermosensitive Phase Behavior and Drug Release of in Situ Gelable Poly ( N -Isopropylacrylamide-Co-Acrylamide ) Microgels. *Colloid Polym. Sci.* **2007**, 515−521.
(54) Zhao, Y.; Zheng, C.; Wang, Q.; Fang, J.; Zhou, G.; Zhao, H.; Yang, Y.; Xu, H.; Feng, G.; Yang, X. Permanent and Peripheral Embolization: Temperature-Sensitive p(n-Isopropylacrylamide-Co-Butyl Methylacrylate) Nanogel as a Novel Blood-Vessel-Embolic Material in the Interventional Therapy of Liver Tumors. *Adv. Funct. Mater.* **2011**, *21*, 2035−2042.
(55) Wang, Q.; Xu, H.; Yang, X.; Yang, Y. Drug Release Behavior from in Situ Gelatinized Thermosensitive Nanogel Aqueous Dispersions. *Int. J. Pharm.* **2008**, *361*, 189−193.
(56) Sitar, S.; Vezočnik, V.; Maček, P.; Kogej, K.; Pahovnik, D.; Žagar, E. Pitfalls in Size Characterization of Soft Particles by Dynamic Light Scattering Online Coupled to Asymmetrical Flow Field-Flow Fractionation. *Anal. Chem.* **2017**, 11744−11752.
(57) Al-manasir, N.; Fanaian, S.; Zhu, K.; Nyström, B.; Karlsson, G.; Kjøniksen, A. Effects of Temperature and PH on the Contraction and Aggregation of Microgels in Aqueous Suspensions. *J. Phys. Chem. B* **2009**, *113*, 11115−11123.
(58) Wu, X.; Pelton, R. H.; Hamielec, aE.; Woods, D. R.; McPhee, W. The Kinetics of Poly(N-Isopropylacrylamide) Microgel Latex Formation. *Colloid Polym. Sci.* **1994**, *272*, 467−477.
(59) Saunders, B. R.; Vincent, B. Microgel Particles as Model Colloids: Theory, Properties and Applications. *Adv. Colloid Interface Sci.* **1999**, *80*, 1−25.
(60) de Kruif, C. G.; van Iersel, E. M. F.; Vrij, A.; Russel, B. W. Hard Sphere Colloidal Dispersions: Viscosity as a Function of Shear Rate and Volume Fraction. *J. Chem. Phys.* **1985**, *83*, 4717−4725.
(61) Wintgens, V.; Amiel, C. Physical Gelation of Amphiphilic Poly(N-Isopropylacrylamide): Influence of the Hydrophobic Groups. *Macromol. Chem. Phys.* **2008**, *209*, 1553−1563.
(62) Chen, S.; Long, J.; Dan, Y. Preparation and Thermal Response Behavior of Poly (N-Isopropylacrylamide-Co-Acrylic Acid) Microgels via Soap-Free Emulsion Polymerization Based on AIBN Initiator. *J. Appl. Polym. Sci.* **2011**, *121*, 3322−3331.
(63) Malkin, A. Y.; Isayev, A. I. 3. Liquids. In *Rheology - Concepts, Methods and Applications*, 2nd ed.; ChemTec, 2012.
(64) Bouhid De Aguiar, I.; Van De Laar, T.; Meireles, M.; Bouchoux, A.; Sprakel, J.; Schroën, K. Deswelling and Deformation of Microgels in Concentrated Packings. *Sci. Rep.* **2017**, *7*, No. 10223.
(65) Andersson, M.; Maunu, S. L. Structural Studies of Poly(N-Isopropylacrylamide) Microgels: Effect of SDS Surfactant Concentration in the Microgel Synthesis. *J. Polym. Sci., Part B: Polym. Phys.* **2006**, *44*, 3305−3314.
(66) Arleth, L.; Xia, X.; Hjelm, R. P.; Wu, J.; Zhibinc, H. U. Volume Transition and Internal Structures of Small Poly(N-Isopropylacrylamide) Microgels. *J. Polym. Sci., Part B: Polym. Phys.* **2005**, *43*, 849−860.
(67) Han, C. K.; Bae, Y. H. Inverse Thermally-Reversible Gelation of Aqueous N-Isopropylacrylamide Copolymer Solutions. *Polymer* **1998**, *39*, 2809−2814.
(68) Yethiraj, A. Tunable Colloids: Control of Colloidal Phase Transitions with Tunable Interactions. *Soft Matter* **2007**, *3*, 1099.



DOI: 10.1021/acs.jpcb.9b04051
*J. Phys. Chem. B* 2019, 123, 6303−6313